RSC Advances

PAPER

View Article Online
View Journal | View Issue

Cite this: *RSC Adv.*, 2021, **11**, 20519

ZEUS (ZIF-based electrochemical ultrasensitive screening) device for isopentane analytics with focus on lung cancer diagnosis†

Ivneet Banga,[a] Anirban Paul,[a] Abha Umesh Sardesai,[a] Sriram Muthukumar [ab] and Shalini Prasad *[ab]

Breath analytics is currently being explored for the development of point-of-care devices in non-invasive disease detection. It is based on the measurement of volatile organic compounds (VOCs) and gases that are produced by the body because of the metabolic pathways. The levels of these metabolites vary due to alteration in the endogenous oxidative stress-related metabolic pathways and can be correlated to understand the underlying disease condition. The levels of exhaled hydrocarbons in human breath can be used to design a rapid, easy to use method for lung cancer detection. This work outlines the development of an electrochemical sensing platform that can be used for the non-invasive diagnosis of lung cancer by monitoring isopentane levels in breath. This electrochemical sensor platform involves the use of [BMIM]BF_4@ZIF-8 for sensing the target analyte. This synthesized nanocomposite offers advantages for gas sensing applications as it possesses unique properties such as an electrochemically active Room Temperature Ionic Liquid (RTIL) and a crosslinking Metal Organic Framework (MOF) that provides increased surface area for gas absorption. This is the first report of a hydrocarbon-based sensor platform developed for lung cancer diagnosis. The developed sensor platform displays sensitivity and specificity for the detection of isopentane up to 600 parts-per-billion. We performed structural and morphological characterization of the synthesized nanocomposite using various analytical techniques such as PXRD, FESEM, FTIR, and DLS. We further analyzed the electrochemical activity of the synthesized nanocomposite using a standard glassy carbon electrode. The application of the nanocomposite for isopentane sensing was done using a commercially available carbon screen printed electrode. The results so obtained helped in strengthening our hypothesis and serve as a proof-of-concept for the development of a breathomics-enabled electrochemical strategy. We illustrated the specificity of the developed nanocomposite by cross-reactivity studies. We envision that the detection platform will allow sensitive and specific sensing of isopentane levels such that it can used for point of care applications in noninvasive and early diagnosis of lung cancer, thereby leading to its early treatment and decrease in mortality rate.

Received 20th April 2021
Accepted 26th May 2021

DOI: 10.1039/d1ra03093k

rsc.li/rsc-advances

Introduction

Breath analysis is emerging as a promising technique for non-invasive disease diagnosis. More than 300 different metabolites are reported to be present in human breath.[1,2] The levels of these compounds in the breath have been correlated to underlying disease conditions such as lung disease, cancer, or inflammation.[3,4] Breathomics is defined as the metabolomics study of exhaled air. It can help in biomarker discovery and serve as a tool for assessing the diseased state of the body and in prognosis.[5] Breathomics is evolving as a rapid, sensitive, specific, and minimally invasive method for studying endogenously produced volatile organic compounds and inorganic gases that are released as a result of metabolic pathways associated with body functions.[6] A relation between levels of biomarkers in breath and lung cancer has been reported by various researchers.[7–9] As lung cancer has a very high mortality rate, it raises the urgency for developing tools that can detect the disease at an early stage. Today, the analysis of breath Volatile Organic Compounds (VOC) holds good promise in the field. Some of the biomarkers associated with lung cancer that are found in the breath include propanol, isoprene, acetone, isopentane, hexanal, toluene, and benzene. One of the pioneer researchers in the field of breathomics, Michael Philips,

[a]*Department of Bioengineering, University of Texas at Dallas, Richardson, Texas 75080, USA. E-mail: ivneetkaur.banga@utdallas.edu; anirban.paul@utdallas.edu; abha.Sardesai@UTDallas.edu; shalini.prasad@utdallas.edu*

[b]*EnLiSense LLC, 1813 Audubon Pond Way, Allen, TX 75013, USA. E-mail: sriramm@enlisense.com*

† Electronic supplementary information (ESI) available. See DOI: 10.1039/d1ra03093k

performed three independent biomarker discovery studies for the detection of lung cancer using GC-MS as the analytical technique.[7,10,11] The results so obtained majorly involved the presence of alkanes that were seen in all three studies. Isopentane levels in breath above 200 parts-per-billion have been reported to be associated with a diseased state. Gordon *et al.* (1985) used gas chromatography mass spectrometry (GC-MS) to study VOCs in exhaled breath.[12] Other studies used proton transfer reaction mass spectrometry (PTR-MS) and ion-mobility spectrometry.[13–15] However, these techniques need sophisticated instrumentation and trained personnel in addition to high cost of equipment and procedure.

For the field monitoring of VOCs, the sensors that are currently being used, are based on the measurement of electrical resistance. As a result, they lack sensitivity and specificity.[16–18] However, researchers have used electrochemical sensors for the detection of various VOCs and gas analytes.[19–22] Moreover, different materials have been explored for the development of electrochemical sensors for VOC detection in breath.[23–29]

Metal Organic Framework (MOF) is a unique porous compound, made of metal ions/cluster and coordinated to organic ligand/fragment which forms one-, two-, or three-dimensional framework. MOFs have widely been explored in the past decade due to their exceptional ability for gas storage, catalysis, and drug delivery.[30–33] Recently, the electrochemical properties of MOF have been explored extensively due to multiple reasons such as its unique design and large surface area along with uniform and tunable pore size.[34] Among zeolitic MOFs, zinc-imidazole framework 8 (ZIF-8) has emerged as a sensing modality due to its unique chemical architecture.

From electrochemical point of view, bare ZIF-8 possesses moderate to low capacitive property but does not have much conductivity, which limits its direct use in electrochemical applications. However, researchers have developed advanced modifications like encapsulation of suitable nanoparticles inside its porous matrix, which help use modified ZIF-8 for various electrochemical applications.[35,36] ZIF-8 has a rough pore size about 3–5 Å and a uniform cavity size of 11–15 Å, which makes it suitable to accommodate small molecules, nanoparticles, ionic liquids, and even biomolecules.[37] This hybridization enhances the composite material to be effective for various applications gas storage, chemical separation, catalysis, drug delivery, and electrochemical sensing.[38–46] In particular, the incorporation of small molecules/nanoparticles in MOF attracts much attention because of the benefits of novel chemical and physical properties exhibited by certain classes of small molecules/nanoparticles.[47–49] One such material is the Room Temperature Ionic Liquid (RTIL) that is a subclass of ionic liquid family, having zwitter ionic structure of cation and anion and is stable at room temperature. Along with unique physicochemical property, it also possesses high thermal stability (up to 300 °C), superior ionic conductivity, as well as excellent electrochemical capacity.[50] Due to this reason, it is known and utilized extensively as electrochemical transducer for electrochemical application.[51,52] Our group has explored the potential of RTIL and its role in an electrochemical platform for the detection of CO_2.[53] There are many other reports where [BMIM]BF_4 has been utilized for gas separation as well as electrochemical application. Encapsulation of such RTIL in MOF matrix will show dual functionality toward gas adsorption and diffusion and can be employed into successive electrochemical gas sensor application. Computational study suggests the stability of RTIL remains intact inside ZIF-8 and RTIL has been used as an encapsulated agent into ZIF-8 matrix. There are other reports where various RTILs have been encapsulated into ZIF-8 matrix for different applications.[54,55] Although there are reports where RTIL encapsulation has been achieved into ZIF-8 matrix, encapsulation of [BMIM]BF_4 has not been reported yet. There are almost no reports of RTIL encapsulated ZIF-8 hybrid material for electrochemical gas sensor application.

In this work, we have synthesized [BMIM]BF_4@ZIF-8 nanocomposite by encapsulation of RTIL (used to allow diffusion of target VOC molecules) in to the ZIF-8 moiety (Scheme 1). We effectively utilized the synthesized nanocomposite for the detection of isopentane levels by using electrochemical transduction mechanism. This work displays the development of handheld sensing platform that serves as a proof-of-concept for noninvasive detection of lung cancer by analyzing isopentane levels in breath of the individual. We performed physicochemical and morphological characterization of the inhouse synthesized nanocomposite [BMIM]BF_4@ZIF-8 using techniques such as PXRD, FESEM, FTIR, and DLS. The nanocomposite is used for detection of isopentane (up to 600 ppb as limit of detection) and displays highly sensitive and specific signal response. The inherent electrochemical properties of the material have been explored using standard glassy carbon electrode (GCE) and application of the material has been shown using carbon screen-printed electrode (DROPSENS) for isopentane sensing. Chronoamperometry was used as transduction principle to determine the dose dependent response on the -[BMIM]BF_4@ZIF-8 modified electrode interface for sensing isopentane levels ranging from 600 ppb to 12 ppm. We have demonstrated the specificity of the nanocomposite toward the target gas by performing cross-reactivity studies. We compiled the data for three replicates with 95% confidence interval in sensor response. The study demonstrates the functionality and utility of an Internet of Things (IoT)-based microelectronic prototype. The developed chemical sensor also serves as a proof

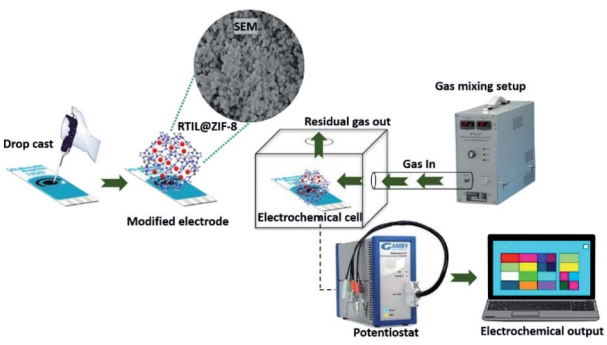

Scheme 1 Schematic representation of the optimized electrochemical sensing approach.

of concept and can be used to develop a robust and sensitive platform for lung cancer detection. The screening device is integrated with [BMIM]BF_4@ZIF-8 modified electrode for the detection of isopentane such that it can used for point of care applications in noninvasive and early diagnosis of lung cancer.

Experimental section

Materials and methods

We purchased analytical grades of chemical such as zinc nitrate, and 2-methylimidazole required for ZIF-8 synthesis from Sigma-Aldrich and used them without further purification. We purchased solvents such as methanol from Sigma-Aldrich and used them without further purification. 0.1 M potassium chloride (KCl) was used as supporting electrolyte for electrochemical sensing application. Ionic liquids such as 1-butyl-3-methylimidazolium tetrafluoroborate [BMIM]BF_4, with over 97% purity, and used for encapsulation inside the ZIF-8 cavity was procured from Milipore Sigma. 1-Ethyl-3-methylimidazolium tetrafluoroborate [EMIM]BF_4 that is used as an electrolyte for carbon screen printed electrode, was also procured from Milipore Sigma. Trace Source™ disposable permeation tube for isopentane was procured from KINTEK analytical. All safety considerations and steps were followed while handling isopentane. We placed the gas dilution setup inside the fume hood. A bubbler setup was preset adjacent to it for discarding any residual gases. While performing the experiments, proper protective equipment was used at all times to ensure that there was no skin and eye contact or accidental inhalation/ingestion.

Synthesis of [BMIM]BF_4@ZIF-8 nanocomposite

The synthesis procedure for [BMIM]BF_4@ZIF-8 was followed stepwise from the previously reported method.[35,56] Two separate solutions of zinc nitrate (labeled as solution A) and 2-methylimidazole (labeled as solution B) were prepared. Zinc nitrate solution with 8 mM concentration was prepared by measuring 2.38 g of the compound and dissolving it into 60 mL methanol. This was labelled as solution A. To this, we added 2.5 mM of BMIM[BF_4]. Solution B was prepared by weighing 2.628 g of 2-methylimidazole and dissolving it in 30 mL of methanol solution. After both the solutions were prepared, we mixed them together in a single beaker and kept it for constant stirring at 600 rpm at room temperature for 10 h. The beaker was kept covered with aluminum foil to avoid evaporation. After few hours of constant stirring, it was observed that the solution turned hazy in nature and the synthesized nanocomposite could be seen settled at the bottom of the beaker. After the process is finished, the solution is allowed to stand overnight and is kept untouched to allow settlement of the nanocomposite. The settled precipitate nanocomposite solution was removed using a 10 mL pipette. The remaining nanocomposite was transferred to a 10 mL centrifuge vial. The solution was centrifuged at 7000 rpm for 10 min. After this step, the solution was washed and resuspended using methanol. This step was repeated five time and the precipitate was removed and resuspended after every washing step. The nanocomposite synthesis after all the washes were complete was collected and stored in glass vials and left to dry overnight under vacuum. The final dried nanocomposite [BMIM]BF_4@ZIF-8 was stored at 4 °C in a dark place.

We analyzed the structural and morphological characteristics of the synthesized nanocomposite using various techniques. PXRD (Powder X-ray Diffraction) was performed using Siemens D500 PXRD to analyze the crystal lattice structure of the synthesized nanocomposite. The morphology of the synthesized nanocomposite was imaged using Field Emission Scanning Electron Microscopy (FESEM) on Hitachi S-3000N SEM/EDS tool. Moreover, the elemental composite of the nanocomposite was determined using EDAX for both ZIF-8 and [BMIM]BF_4@ZIF-8. FT-IR measurements were taken using Nicolet iS-50 FTIR (Thermo Scientific Inc.) in transmittance mode for BMIM[BF_4], ZIF-8 and [BMIM]BF_4@ZIF-8. Dynamic light scattering measurements were taken to determine the hydrodynamic diameter of the synthesized nanocomposite using Malvern Zetasizer Nano ZS (Malvern Instruments, UK).

Electrode modification and characterization using synthesized nanocomposite

The synthesized nanocomposite, [BMIM]BF_4@ZIF-8 was characterized using electrochemical method of transduction. Standard three electrode, glassy-carbon electrode (GCE) was employed and 0.1 M potassium chloride (KCl) was used as the supporting electrolyte. The three electrode setup involves glassy carbon having 3 mm diameter to be used as the working electrode (WE), while reference electrode (RE) made of Ag/AgCl (sat. KCl) and platinum wire forms the counter electrode (CE). This setup was procured from CH instruments. The nanocomposite is dissolved in methanol solution by weighing 1 mg and dispersing it in 200 μL so as to form a slurry. The prepared slurry is then sonicated for 15 min to have a uniform suspension. [BMIM]BF_4@ZIF-8 is used for electrochemical sensing application and ZIF-8 (parent compound) is used as a control compound. ZIF-8 is also weighed and suspended in the similar fashion. After the uniform slurry is formed, the nanocomposite is drop casted on the GCE by placing the electrode in an upward fashion and drop casting 10 μL onto the electrode surface. The electrode is held in upright manner for 15 min and allowed to dry at room temperature resulting in the formation of a thin film. The surface modified GCE is then used for nanocomposite material characterization using electrochemical transduction mechanisms. Cyclic voltammetry (CV), chronoamperometry (CA), and chronocoulometry (CC) was performed. For CV, the parameters were selected as follows: potential in the range of 0 V to +1.2 V *vs.* Ag/AgCl (sat. KCl) with a scan rate of 50 mV s^{-1}. Scan rate was varied from 25 mV s^{-1} to 250 mV s^{-1} to understand the capacitive nature of the synthesized nanocomposite material. Diffusion characteristics of the system were studied using double potential chronoamperometry. Double step potential was applied, that is +0.6 V for 30 s and −0.6 V for 30 s. Additionally, chronocoulometry was also performed by applying the same potential conditions. The application of the

synthesized nanocomposite for sensing isopentane was demonstrated using carbon SPE (DROPSENS). The carbon SPE has working electrode (WE) and counter electrode (CE), both made up of carbon, and the WE has diameter as 4 mm. The reference electrode is made of Ag/AgCl. The sensors were procured from Metrohm Dropsens USA. In the carbon SPE, the WE was modified with the nanocomposite material by drop casting 5 μL of the nanocomposite material ([BMIM]BF_4@ZIF-8). The three-electrode setup requires an electrolyte to form connection between all three electrodes and serve as a transducer. For this purpose, we used 1-ethyl-3-methylimidazolium tetrafluoroborate (EMIM[BF_4]) as the electrolyte by drop casting 50 μL of the RTIL such that it covers the entire electrode surface area. For generation of isopentane in the vapor phase VOC, we used Trace Source™ disposable permeation tube, which was procured from KINTEK analytical. We followed proper safety considerations while performing experiments and working with the gas sensing setup. The setup was placed inside the fume hood and inhouse nitrogen supply was used as a diluent gas for the gas mixing. The electrochemical gas sensing setup that was attached to the mixing setup has a bubbler system present for gas disposal. The sensing setup has been depicted in Fig. S1.† Chronoamperometry was used as the transduction mechanism to study to dose dependent response of the nanocomposite modified electrode to isopentane levels ranging from 600 ppb to 12 ppm. Electrochemical Impedance Spectroscopy (EIS) was used to understand the capacitive behavior of electrode–electrolyte interface upon interaction with the target gas. Electrochemical characterizations were performed using Gamry series 600 potentiostat/galvanostat. Demonstration of proof-of-concept prototype was done using the Emstat pico development board, developed by PalmSens and Analog Devices. It is a small form factor potentiostat that includes a ADuCM355 microcontroller. The nanocomposite material modified electrode was soldered with the development board and the entire device was enclosed in a 3D design that was printed using the Form-labs Form 2 3D printer. The handheld sensing prototype was used for sensing isopentane for mainly three concentrations, 600 ppb, 4 ppm, and 12 ppm. The prototype *via* bluetooth connectivity and the data was stored to google sheets from where the designed WebApp extracts the transient diffusion current and displays the results.

Results and discussion

Characterization of the synthesized nanocomposite using various physicochemical techniques

The synthesized nanocomposite [BMIM]BF_4@ZIF-8 possesses characteristic structural features due to the parent compound, that is ZIF-8, which forms the backbone of the nanocomposite. The nanocomposite was analyzed using different physicochemical techniques to study the surface morphological features. The nanocomposite material was dried under vacuum and was used for PXRD analysis for phase characterization. The pattern so obtained for [BMIM]BF_4@ZIF-8 (black line) nanocomposite and ZIF-8 (used as control compound) has been depicted in Fig. 1. The PXRD result depicts the presence of almost all major planes of bare ZIF-8 into [BMIM]BF_4@ZIF-8, suggesting no structural deformity due to the encapsulation of RTIL inside the ZIF-8 moiety. As RTIL is liquid in its bare state, no characteristic peak of RTIL is identified in PXRD pattern, indicating that RTIL is uniformly dispersed in bulk-[BMIM]BF_4@ZIF-8 at a molecular level. The standard peaks of the parent synthesized ZIF-8 are also compared to simulated ZIF-8 (JCPDS 00-062-1030; $a = b = c = 17.0116$ Å $\alpha = \beta = \gamma = 90°$) and depicted in Fig. S2 ESI.† The major phase peaks of the parent synthesized ZIF-8 compound completely match with the simulated ZIF-8, hence, suggesting the purity of the synthesized crystal structure of ZIF-8. This observation suggests that the synthesized hybrid MOF-RTIL microstructure, [BMIM]BF_4@ZIF-8, maintains the crystal lattice cubic structure of ZIF-8 even after encapsulation of RTIL. The cubic crystal structure of the synthesized [BMIM]BF_4@ZIF-8 is also consistent with the FESEM observation, which strengthens our hypothesis of encapsulation of RTIL inside ZIF-8.

The morphological characterization of the synthesized nanocomposite, [BMIM]BF_4@ZIF-8 was done using FESEM. Fig. 2 denotes a FESEM surface morphology characteristic of the [BMIM]BF_4@ZIF-8 at different magnifications. Fig. 2a represents an agglomerated homogenous cubic crystal structure of the [BMIM]BF_4@ZIF-8 at low magnification. On further increase in magnification (Fig. 2b and c), we observe the presence of units of cubic crystal lattice structures. Finally, at highest magnification and by focusing on one cubic crystal structure, we observe the highly magnified FESEM image (Fig. 2d). The native morphology of the pure ZIF-8 has been reported as cubic crystal.[35] It has also been reported in literature that on modification of ZIF-8 by incorporation of different nanostructures, the native structure of the parent compound remains intact. The encapsulation of RTIL inside the ZIF-8 should not disrupt the morphology of parent compound, that is pure ZIF-8.[36,57] The result also aligns with PXRD result that strengthens our hypothesis for its cubic shaped morphology. Therefore, the FESEM images so obtained suggest that the morphology of ZIF-8 remains intact after the incorporation of the ionic liquid inside the lattice of the ZIF-8 and is in coordination with the literature studies.

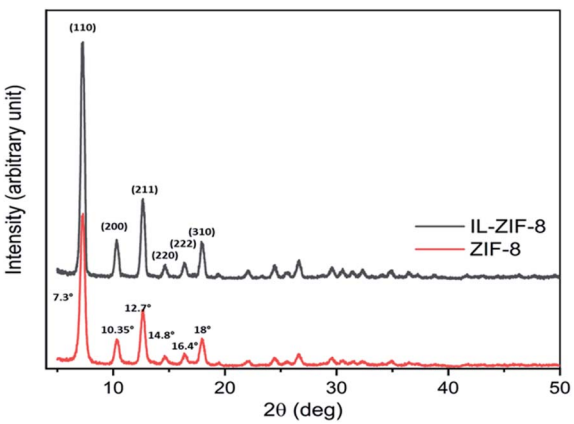

Fig. 1 PXRD patterns for the synthesized nanocomposite [BMIM]BF_4@ZIF-8 (black line) and ZIF-8 (red line) only.

Uniform distribution of the RTIL inside the nanocomposite is studied using energy dispersive X-ray analysis (EDAX) for both [BMIM]BF_4@ZIF-8 hybrid and ZIF-8 parent compound. Both the structures have C, N, Zn, and O uniformly present. This supports our hypothesis that RTIL is successfully incorporated inside the ZIF-8 moiety. The EDX spectra and the elemental composition of the synthesized nanocomposite as well as ZIF-8 is depicted in Fig. S3 ESI.†

The chemical structure of the synthesized [BMIM]BF_4@ZIF-8 was characterized using Fourier Transform Infrared (FT-IR) spectroscopy to analyze the interaction and encapsulation of RTIL inside ZIF-8 motif. FT-Infrared (IR) spectroscopy was done using Nicolet iS-50 FTIR (Thermo Scientific Inc.) in Transmittance mode. The IR spectra was collected using Germanium crystal for 256 scans at a resolution of 4 cm^{-1} in the wavelength range 500 cm^{-1} to 4000 cm^{-1}. Three samples were analyzed, in which ZIF-8 and [BMIM]BF_4@ZIF-8 are powdered in nature, when placed under crystal. FT-IR of bare RTIL is measured by forming a thin film of RTIL onto a glass slide. See Fig. 3 for the IR spectra, with blue line representing spectra for RTIL, black line for ZIF-8, and red line for [BMIM]BF_4@ZIF-8. That the figure shows that almost all major fingerprint FT-IR peaks of bare ZIF-8 are present in the [BMIM]BF_4@ZIF-8 – at 3135 cm^{-1} (aromatic C–H asymmetric stretching vibrations), 1585 cm^{-1} (C=N stretching vibration), 1458 cm^{-1} (depicts entire ring stretching), and 1148 cm^{-1} (aromatic C–N stretching mode). Similarly, the peaks at 997 cm^{-1} and 752 cm^{-1} can be assigned as C–N bending vibrations and C–H bending modes respectively. The signature peaks of ZIF-8 can be seen in the synthesized nanocomposite spectra, indicating that there is no chemical deformation of the inherent ZIF-8 backbone. The FT-IR of bare RTIL spectra has all the major peaks, but the peaks are not visible in [BMIM]BF_4@ZIF-8 hybrid structure, indicating successful infusion or encapsulation of RTIL onto ZIF-8 matrix without deforming ZIF-8's native structure.[37]

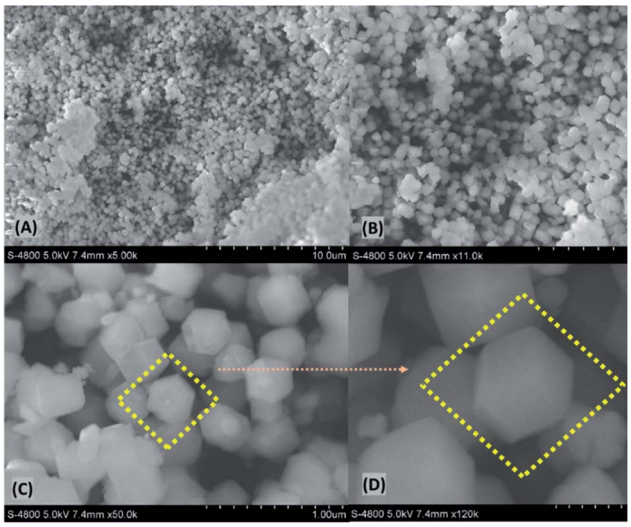

Fig. 2 FESEM images of [BMIM]BF_4@ZIF-8 nanocomposite. Scale bars: (a) 10 μm, (b) 5 μm, (c) 1 μm, (d) 0.4 μm.

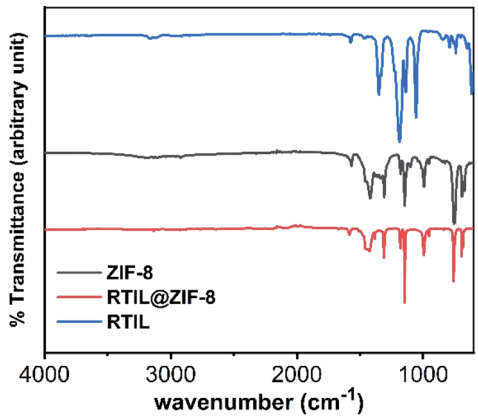

Fig. 3 FTIR spectra of [BMIM]BF_4 (black line), ZIF-8 (red line), and [BMIM]BF_4@ZIF-8 (blue line).

Furthermore, the hydrodynamic diameter of the synthesized nanocomposite was characterized using dynamic light scattering (DLS) analysis (Fig. S4 ESI†). The diameter of the parent compound, ZIF-8 was found to be 214 ± 7.2 nm. According to literature, the average particle size for ZIF-8 is reported as approximately 200 nm and thus, supports our experimental results.[37] On incorporation of RTIL inside the ZIF-8 moiety, the hydrodynamic diameter increased to 1097 ± 6.7 nm, and hence, supports our hypothesis that RTIL resides inside the ZIF-8 cavity.

Characterization of the synthesized nanocomposite [BMIM]BF_4@ZIF-8 using standard GCE by application of electrochemical transduction techniques

The synthesized nanocomposite was characterized using DC-based transduction technique. The WE has been modified by drop casting the material onto the sensor surface. The modified GCE was then immersed in an 0.1 M KCl solution. Cyclic voltammetry measurement was carried out in the range of 0 V to 1.0 V with a scan rate of 100 mV s^{-1}. The measurement was performed for bare electrode, [BMIM]BF_4@ZIF-8 and ZIF-8 and the graph so obtained is depicted in Fig. 4a. For the bare electrode, we observed that there was no diffusion. On the other

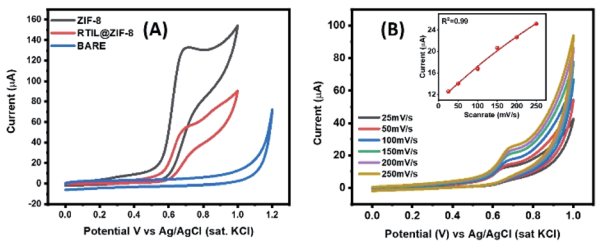

Fig. 4 Electrochemical characterization of [BMIM]BF_4@ZIF-8 using standard GCE setup (a) cyclic voltammograms of [BMIM]BF_4@ZIF-8 and ZIF-8 in 0.1 M KCl. (b) Scan rate variation study using [BMIM]BF_4@ZIF-8 modified GCE. Peak current plotted with scan rate to validate Randles–Sevcik equation, showing strong correlation between the two parameters.

hand, the graph depicts typical non-faradaic nature of the nanocomposite ([BMIM]BF_4@ZIF-8) as well as the parent compound, ZIF-8. This behavior can be attributed to the double layer capacitance and the absence of redox species that can cause charge transfer across the electrode–electrolyte interface. We varied the scan rate from 25 mV s^{-1} to 250 mV s^{-1} to understand the double layer modulation and get a better understanding of the capacitive nature of the nanocomposite. The result is shown in Fig. 4b and the inset of the figure shows linear correlation between scan rate and peak current having a R^2 of 0.99. The cyclic voltammogram shows that the increase in scan rate correlates to an increase in peak current and follows the famous Randles–Sevcik equation (eqn (1)).

$$i_p = 0.4463nFAC\sqrt{\left(\frac{nF\theta D}{RT}\right)} \quad (1)$$

where all the terms denote their usual meaning.

The diffusion behavior of the nanocomposite was characterized using double potential chronoamperometry. Double step potential was applied, that is +0.6 V for 30 s and −0.6 V for 30 s. The chronoamperograms curves have been depicted in Fig. 5a with the cathodic and anodic currents at 5 s shown in the inset of the graph. Furthermore, the capacitive behavior of the nanocomposite was studied using chronocoulometry (Fig. 5b). The charging and discharging cycles were recorded at +0.6 V for 30 s and −0.6 V for 30 s respectively. The results support our hypothesis that the synthesized nanocomposite possesses excellent capacitive behavior and is reversible in nature as can be seen in the charging–discharging cycles.

ZIF-8 possesses unique pore structure, with an approximate pore size of 3.4 Å and cavity size of approximate 11 Å.[35] On the contrary, [BMIM][BF_4] is a viscous compound having molecular weight of 226 g mol^{-1}. As it is viscous in nature, it does not have distinct molecular size, but due to high ionic conductivity and zwitter ionic alike chemical structure, it prefers non-covalent interaction along with conventional –H bonding. This provides the driving force for RTIL to be encapsulated onto ZIF-8 matrix. Along with physico-chemical property of bare ZIF-8, the hybrid composite consists of suitable adsorption and electrochemical property which enables the composite material to mediate electrons. This will allow easy and rapid diffusion of the target gas analyte across the modified electrode interface.

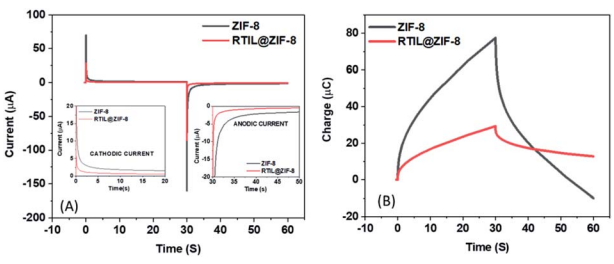

Fig. 5 Electrochemical characterization of [BMIM]BF_4@ZIF-8 using standard GCE (a) double potential chronoamperometry scan was performed for [BMIM]BF_4@ZIF-8 and ZIF-8 (b) chronocoulometric characterization of [BMIM]BF_4@ZIF-8 and ZIF-8 showing capacitive behavior of the nanocomposite.

The synthesized hybrid nanocomposite has dual properties, such that ZIF-8 allows the physisorption of target gas species even in low concentration and RTIL acts as a transducer for electrochemical detection.

Application of the nanocomposite for detection of isopentane as a biomarker for lung cancer

The results obtained from the synthesized nanocomposite using the standard GCE helped in understanding the electrochemical nature of the nanocomposite. Therefore, the material was used for the detection of isopentane as a biomarker for lung cancer. Electrochemical transduction mechanism is used for the development of Point of Care (PoC) platforms as they are robust, sensitive and specific in nature especially for gas and VOC sensing applications.[19,21,53,58] We used commercially available carbon SPE as the electrode system for sensing application as it can be easily integrated into a microelectronics platform. The electrode design involves concentric three electrode system wherein the WE and the CE are made of carbon and the RE is made of Ag/AgCl. The WE has been modified by drop casting the synthesized nanocomposite on the sensor surface at a fixed concentration 1 mg dispersed in 200 μL methanol). The sensor surface was allowed to dry at room temperature so as to form a thin film on the electrode. In a three-electrode design, we require an electrolyte that covers the entire electrode surface and helps completing the circuit for electrochemical transduction. In this application, we used [EMIM][BF_4] as the electrolyte by drop casting 50 μL on the electrode surface. RTIL are widely used as electrolytes for gas sensing applications as they allow easy diffusion of the target gas species across the electrode–electrolyte interface. Cyclic voltammetry was performed in the presence of the target gas to understand the gas diffusion characteristics and capacitive nature of the electrode–electrolyte interface. CV measurements were taken from −1 V to +1 V with varying the scan rate from 25 mV s^{-1} to 250 mV s^{-1} for detection of isopentane at 600 ppb concentration level. The cyclic voltammograms so obtained show purely capacitive nature of the electrode–electrolyte interface and hence supports our hypothesis. The graphs so obtained have been depicted in Fig. S5 ESI.† The diffusion limited behavior of the [BMIM]BF_4@ZIF-8 modified electrode system is characterized using chronoamperometry.

The modified electrode–electrolyte interface behaves as a semi-permeable membrane and creates a concentration gradient at the interface to allow diffusion of the target gas analyte. The equation of Fick's law of diffusion is as follows

$$J = -D\frac{\partial C}{\partial x} \quad (2)$$

where J is the diffusion flux, D is the diffusion coefficient, x is the position, and C is the concentration.

For studying diffusion characteristics using chronoamperometry as the transduction principle, we use the Cottrell equation as follows

$$i = \frac{nFAc_j^0\sqrt{D_j}}{\sqrt{\pi t}} \quad (3)$$

where, i is the current due to diffusion, c_j^0 is the concentration of the diffused species, and t is time.

Chronoamperometric measurement was performed to record the cathodic current as a result of the diffusion of the isopentane molecules across the electrode–electrolyte interface. To record transient diffusion current, chronoamperometry was recorded at +0.6 V for 30 s. The chronoamperogram so obtained was plotted and depicted in Fig. 6. The inset of the figure depicts the transient cathodic diffusion current at 5 s with increasing concentration. This transient current depicts the dynamic gas diffusion phenomenon across the electrode–electrolyte interface before the system reaches a steady state. Linear fitting was done to analyze the calibrated dose response for 0.6 ppm to 12 ppm (Fig. S6 ESI†) and R^2 value of greater that 0.92 was obtained for both lower concentrations (0.6–4 ppm) and higher concentration (4–12 ppm) range. Also, the limit of detection (LOD) as 600 ppb was statistically calculated and was significantly greater (3σ) from the baseline value (Fig. S7 ESI†). It was calculated using the formula

$$\mathrm{LOD} = 3\sigma/S \quad (4)$$

where σ stands for standard deviation and S stands for slope of the calibration curve.

The modified electrode with [BMIM]BF_4@ZIF-8 and EMIM [BF_4] as the electrolyte, serves as an excellent electrochemical platform for sensing isopentane as a biomarker of lung cancer. The electrochemical characterization was performed for isopentane levels ranging from 600 ppb to 12 ppm. The chronoamperogram so obtained show that the sensor system has linear response to the target gas concentration. This dose dependent response supports our hypothesis that the modified electrode system can be used for isopentane sensing and be applied for PoC diagnosis. The result also indicates significant amount of diffusion of the target analyte across the electrode electrolyte interface. This diffusion analytics is also seen prevalent in EIS characterization. This system is unique in the sense that it displays high ionic charge conductivity owing to the synthesized nanocomposite as it allows easy charge transfer and diffusion. The data reported in Fig. 6 has been compiled and analyzed for three replicates and the dose dependent response has been represented with 5% error bar.

The electrochemical mediated diffusion behavior of the [BMIM]BF_4@ZIF-8 modified electrode is explored using electrochemical impedance spectroscopy (EIS). AC frequency perturbation to the developed electrochemical interface aids in understanding the diffusion limited behavior and capacitive response of the sensor. Our group has previously established and validated the use of EIS to understand the gas diffusion phenomenon using the interdigitated electrode modified with RTIL.[19,20,53] We leveraged similar concept in our experiment and performed EIS in a frequency range of 1 MHz–0.1 Hz. The corresponding Nyquist plot is represented in Fig. 7 for low, medium, and high concentrations. The associated Bode plot is depicted in Fig. S8 ESI.† The Nyquist plot so obtained clearly shows that there is absence of charge transfer along the electrode–electrolyte interface, but presence of a capacitance driven bulk diffusion output is also shown as Warburg diffusion. This capacitive nature can be attributed to the presence of RTIL in the nanocomposite. The Bode plot depicts variation in both Z mod as well as phase angle with respect to increase in concentration of isopentane levels. RTIL present in this electrochemical system acts as both transducer and electrolyte. It was observed that DC-based chronoamperometry technique monitors the current due to diffusion phenomenon, and EIS depicts the diffusion profile not due to any faradic charge transfer phenomenon but can be attributed to bulk diffusion of isopentane through [BMIM]BF_4@ZIF-8.

Characterization of [BMIM]BF_4@ZIF-8 nanocomposite response in the presence of cross-reactive gases

The selective and specific sensing response of the novel synthesized nanocomposite for detection of isopentane over other environmental gases and VOCs that are existing as cross-

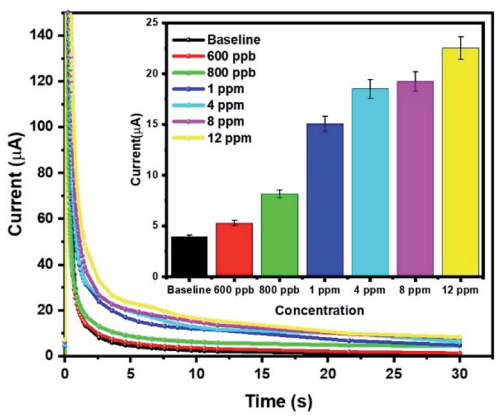

Fig. 6 Diffusion limited chronoamperometry response curve. Chronoamperometry measurement was taken at 0.6 V for 30 s on the [BMIM]BF_4@ZIF-8 modified electrode for sensing isopentane levels ranging from 600 ppb to 12 ppm.

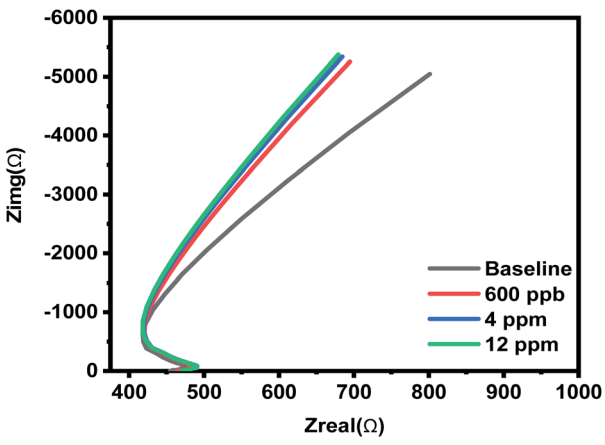

Fig. 7 EIS-based analysis for [BMIM]BF_4@ZIF-8 modified electrode–electrolyte interface for isopentane sensing for low, medium, and high levels. Nyquist plot showing the curve so obtained for different levels of target gas.

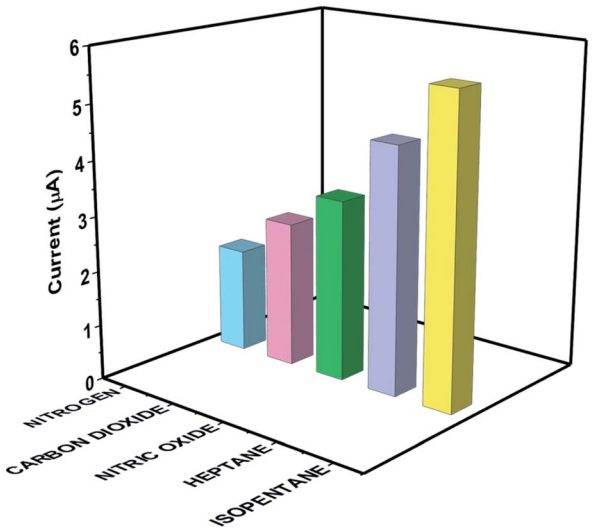

Fig. 8 Selectively and specific sensing response of the [BMIM]BF_4@ZIF-8 modified electrode for detection of isopentane over other gases and volatile chemical compounds, including nitrogen, carbon dioxide, nitric oxide, heptane, and isopentane.

reactive molecules was determined. The selective sensing response of the target analyte isopentane at 600 ppb as equated to nitrogen, carbon dioxide, nitric oxide, and heptane is depicted in Fig. 8. The [BMIM]BF_4@ZIF-8 modified electrode displays a specific and selective chronoamperometry response for isopentane sensing. The average transient diffusion cathodic current at 5 s and 0.6 V is depicted in Fig. 8. The specific signal for isopentane was found to be 5.59 μA and the average non-specific signal for cross-reactive gases and VOC was 1.98 μA, which is assessed to be thrice larger signal as compared to the non-specific signal.

Translatability of the [BMIM]BF_4@ZIF-8 nanocomposite modified electrode system toward portable microelectronic prototype development to demonstrate on-field applicability

The results from benchtop experiments using standard potentiostat setup have been analyzed and used for the development of miniaturized form factor prototype for PoC application. For this purpose, a handheld research device integrated with an IoT based platform was designed and fabricated, such that it can detect three different levels (low, medium and high) of isopentane concentrations to be able to provide actionable and useful data about the disease diagnosis. The prototype device depicted in Fig. 9a comprises of [BMIM]BF_4@ZIF-8 modified electrode coupled with Emstat pico development board. Fig. 9a represents the sensing scheme involved using the prototype device. CA has been performed at 0.6 V for three different concentrations of isopentane: 600 ppb (LOD), 4 ppm (medium) and 12 ppm (high). After the exposure of the prototype to the target analyte concentration, the software is run on the screening device and the output data is stored on google sheets. The transient diffusion current is then extracted using the developed

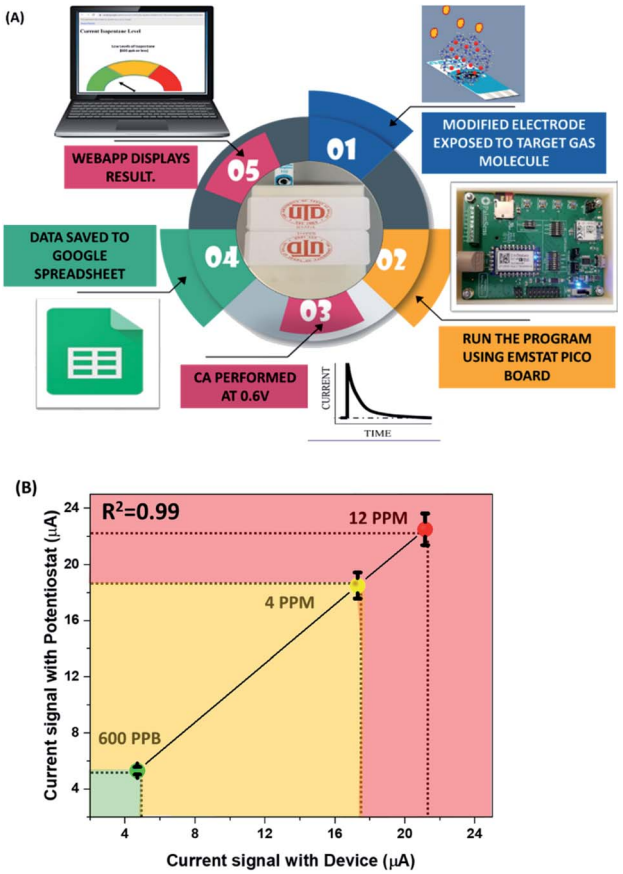

Fig. 9 (a) Diagram representing the working scheme of research prototype comprising of BMIM]BF_4@ZIF-8 modified electrode connected to Emstat pico board and results displayed *via* the WebApp. (b) Dose dependent response of prototype device (*x*-axis) studied against that of lab instrument (*y*-axis) for isopentane: 600 ppb (low), 4 ppm (medium) and 12 ppm (high).

WebApp. The transient diffusion current at 5 s is used to classify the sensor response to three categories – low (green-600 ppb), medium (yellow-4 ppm), or high concentration (red-12 ppm). The result is displayed on the webpage. We also compared the output current from the prototype device to the standard benchtop potentiostat (Gamry) and the result is depicted in Fig. 9b. The CA signal correlation obtained for the transient diffusion current at 5 s for the two devices, shows a linear correlation relation having R^2 of 0.99. This strengthens our hypothesis that fabricated IoT platform can be used for healthcare applications.

Conclusion

Breath analytics is a promising methodology for non-invasive diagnosis of lung cancer. However, no sensor platform has been developed so far that can allow consistent, robust, sensitive, and specific diagnostic response, with potential to be applied for PoC applications. This is the first proof-of-concept of a handheld, IoT-based microelectronic platform for rapid and dynamic detection of isopentane levels. Hydrocarbon levels, such as

those of isopentane, can be used as a biomarker for simple and real-time monitoring of lung cancer. We synthesized [BMIM]BF_4@ZIF-8 nanocomposite to be used as a transducing element for electrochemical detection. This nanocomposite was characterized for morphological and structural features using various analytical techniques. We performed FESEM, FTIR, and DLS for both [BMIM]BF_4@ZIF-8 and ZIF-8 (control compound) to analyze the physico-chemical properties of the synthesized nanocomposite. Electrochemical characterization of the nanocomposite was done using standard glassy carbon electrode and its application for lung cancer detection was explored using commercially available glassy carbon electrode that can be easily integrated into a microelectronic platform. The presented work demonstrates sensing capability up to 600 ppb as the level of detection with high specificity and sensitivity in sensor performance. Chronoamperometry was used as the transduction method to determine the dose-dependent response of the nanocomposite modified electrode interface. The high ionic charge conductivity of the system can be attributed to RTIL incorporated inside the ZIF-8 moiety. The nanocomposite having RTIL and ZIF-8 together makes the system electrochemically active and allows easy diffusion of the target analyte across the electrode–electrolyte interface. We observed a linear dose dependent response of the sensor platform toward increasing concentration of isopentane. The results so obtained support our hypothesis that the developed electrochemical platform is mediated by diffusion phenomenon and can be used for sensing in the lower ppb range. The interaction of isopentane with the electrode–electrolyte interface was also studied using AC-based technique. EIS provided insights into the capacitive behavior of the system because of bulk diffusion of isopentane across the electrode–electrolyte interface. The specificity studies for the system were carried by performing cross-reactivity measurements. We demonstrate the proof-of-concept of an electrochemical sensor platform using [BMIM]BF_4@ZIF-8 as the transducing element that can be incorporated into a PoC microelectronic platform for non-invasive sensing. We envision that the developed platform can help in early detection of lung cancer, thus leading to its early treatment and a significant decrease in mortality.

Author contributions

S. P., S. M., I. B. and A. P. conceived the theoretical framework of the detection scheme and design of experiments. I. B. performed the sensor functionalization used in the experiments. I. B. performed the experiments. I. B. and A. P. analyzed the experimental data and drafted the paper. A. S. helped in the development of the WebApp.

Conflicts of interest

Shalini Prasad and Sriram Muthukumar has a significant interest in EnLiSense LLC, a company that may have a commercial interest in the results of this research and technology. The potential individual conflict of interest has been reviewed and managed by The University of Texas at Dallas and played no role in the study design; in the collection, analysis, and interpretation of data; in the writing of the report; or in the decision to submit the report for publication.

Acknowledgements

I. B. and A. P. acknowledge Mr Vikram Narayanan Dhamu for his help and support.

References

1 M. Phillips, J. Herrera, S. Krishnan, M. Zain, J. Greenberg and R. N. Cataneo, *J. Chromatogr. B: Biomed. Sci. Appl.*, 1999, **729**, 75–88.
2 S. M. Gordon, J. P. Szidon, B. K. Krotoszynski, R. D. Gibbons and H. J. O'Neill, *Clin. Chem.*, 1985, **31**, 1278–1282.
3 B. Buszewski, M. Kęsy, T. Ligor and A. Amann, *Biomed. Chromatogr.*, 2007, **21**, 553–566.
4 W. Miekisch, J. K. Schubert and G. F. E. Noeldge-Schomburg, *Clin. Chim. Acta*, 2004, **347**, 25–39.
5 A. Smolinska, A.-C. Hauschild, R. Fijten, J. Dallinga, J. Baumbach and F. Van Schooten, *J. Breath Res.*, 2014, **8**, 27105.
6 A. W. Boots, J. J. B. N. van Berkel, J. W. Dallinga, A. Smolinska, E. F. Wouters and F. J. van Schooten, *J. Breath Res.*, 2012, **6**, 27108.
7 M. Phillips, R. N. Cataneo, A. R. C. Cummin, A. J. Gagliardi, K. Gleeson, J. Greenberg, R. A. Maxfield and W. N. Rom, *Chest*, 2003, **123**, 2115–2123.
8 M. Phillips, N. Altorki, J. H. M. Austin, R. B. Cameron, R. N. Cataneo, R. Kloss, R. A. Maxfield, M. I. Munawar, H. I. Pass, A. Rashid, W. N. Rom, P. Schmitt and J. Wai, *Clin. Chim. Acta*, 2008, **393**, 76–84.
9 M. Ligor, T. Ligor, A. Bajtarevic, C. Ager, M. Pienz, M. Klieber, H. Denz, M. Fiegl, W. Hilbe, W. Weiss, P. Lukas, H. Jamnig, M. Hackl, B. Buszewski, W. Miekisch, J. Schubert and A. Amann, *Clin. Chem. Lab. Med.*, 2009, **47**, 550–560.
10 M. Phillips, N. Altorki, J. H. M. Austin, R. B. Cameron, R. N. Cataneo, J. Greenberg, R. Kloss, R. A. Maxfield, M. I. Munawar, H. I. Pass, A. Rashid, W. N. Rom and P. Schmitt, *Cancer Biomarkers*, 2007, **3**, 95–109.
11 M. Phillips, R. N. Cataneo, A. R. C. Cummin, A. J. Gagliardi, K. Gleeson, J. Greenberg, R. A. Maxfield and W. N. Rom, *Chest*, 2003, **123**, 2115–2123.
12 H. J. O'Neill, S. M. Gordon, M. H. O'Neill, R. D. Gibbons and J. P. Szidon, *Clin. Chem.*, 1988, **34**, 1613–1618.
13 T. Feinberg, L. Alkoby-Meshulam, J. Herbig, J. C. Cancilla, J. S. Torrecilla, N. Gai Mor, J. Bar, M. Ilouze, H. Haick and N. Peled, *J. Breath Res.*, 2016, **10**, 26012.
14 H. Handa, A. Usuba, S. Maddula, J. I. Baumbach, M. Mineshita and T. Miyazawa, *PLoS One*, 2014, **9**, e114555.
15 A. Bajtarevic, C. Ager, M. Pienz, M. Klieber, K. Schwarz, M. Ligor, T. Ligor, W. Filipiak, H. Denz, M. Fiegl, W. Hilbe, W. Weiss, P. Lukas, H. Jamnig, M. Hackl, A. Haidenberger, B. Buszewski, W. Miekisch, J. Schubert and A. Amann, *BMC Cancer*, 2009, **9**, 348.

16 X. Zang, X. Wang, Y. Jiang, X. Wang, Z. Yang, J. Cong, J. Chen, J. Ji, C. Lu and M. Xue, *Adv. Funct. Mater.*, 2017, **27**, 1702706.
17 M. Xue, F. Li, D. Chen, Z. Yang, X. Wang and J. Ji, *Adv. Mater.*, 2016, **28**, 8265–8270.
18 H. Yan, M. Zhong, Z. Lv and P. Wan, *Small*, 2017, **13**, 1701697.
19 I. Banga, A. Paul, A. U. Sardesai, S. Muthukumar and S. Prasad, *Electrochim. Acta*, 2021, **368**, 137624.
20 A. Bhide, B. Jagannath, E. Graef and S. Prasad, *ECS J. Solid State Sci. Technol.*, 2018, **7**, Q3043–Q3048.
21 E. W. Graef, B. Jagannath, R. Munje and S. Prasad, *IEEE Sens. J.*, 2018, **18**, 3517–3523.
22 E. W. Graef, R. D. Munje and S. Prasad, *IEEE Trans. Nanotechnol.*, 2017, **16**, 826–831.
23 P. I. Gouma, *Proceedings IMCS*, AMA Service GmbH, Von-Münchhausen-Str. 49, 31515 Wunstorf, Germany, 2018, pp. 55–56.
24 G. Jiang, M. Goledzinowski, F. J. E. Comeau, H. Zarrin, G. Lui, J. Lenos, A. Veileux, G. Liu, J. Zhang, S. Hemmati, J. Qiao and Z. Chen, *Adv. Funct. Mater.*, 2016, **26**, 1729–1736.
25 T. R. L. C. Paixão and M. Bertotti, *J. Electroanal. Chem.*, 2004, **571**, 101–109.
26 M. Arvani, H. Mohammad Aliha, A. A. Khodadadi and Y. Mortazavi, *Sci. Iran.*, 2017, **24**, 3033–3040.
27 E. M. Gaffney, K. Lim and S. D. Minteer, *Curr. Opin. Electrochem.*, 2020, **23**, 26–30.
28 E. Bihar, Y. Deng, T. Miyake, M. Saadaoui, G. G. Malliaras and M. Rolandi, *Sci. Rep.*, 2016, **6**, 27582.
29 L. Wang, K. Kalyanasundaram, M. Stanacevic and P. Gouma, *Sens. Lett.*, 2010, **8**, 709–712.
30 J. Han, M. Zhang, G. Chen, Y. Zhang, Q. Wei, Y. Zhuo, G. Xie, R. Yuan and S. Chen, *J. Mater. Chem. B*, 2017, **5**, 8330–8336.
31 P. Lama, H. Aggarwal, C. X. Bezuidenhout and L. J. Barbour, *Angew. Chem., Int. Ed. Engl.*, 2016, **55**, 13271–13275.
32 K. Adil, Y. Belmabkhout, R. S. Pillai, A. Cadiau, P. M. Bhatt, A. H. Assen, G. Maurin and M. Eddaoudi, *Chem. Soc. Rev.*, 2017, **46**, 3402–3430.
33 U. Mueller, M. Schubert, F. Teich, H. Puetter, K. Schierle-Arndt and J. Pastré, *J. Mater. Chem.*, 2006, **16**, 626–636.
34 H. Furukawa, K. E. Cordova, M. O'Keeffe and O. M. Yaghi, *Science*, 2013, **341**, 1230444.
35 A. Paul, G. Vyas, P. Paul and D. N. Srivastava, *ACS Appl. Nano Mater.*, 2018, **1**, 3600–3607.
36 A. Paul and D. N. Srivastava, *ACS Omega*, 2018, **3**, 14634–14640.
37 J. Wang, G. Han, L. Wang, L. Du, G. Chen, Y. Gao, Y. Ma, C. Du, X. Cheng, P. Zuo and G. Yin, *Small*, 2018, **14**, 1704282.
38 H. Zhong, J. Wang, Y. Zhang, W. Xu, W. Xing, D. Xu, Y. Zhang and X. Zhang, *Angew. Chem., Int. Ed.*, 2014, **53**, 14235–14239.
39 Y. Pan, Y. Liu, G. Zeng, L. Zhao and Z. Lai, *Chem. Commun.*, 2011, **47**, 2071–2073.
40 G. Lu and J. T. Hupp, *J. Am. Chem. Soc.*, 2010, **132**, 7832–7833.
41 R. Banerjee, H. Furukawa, D. Britt, C. Knobler, M. O'Keeffe and O. M. Yaghi, *J. Am. Chem. Soc.*, 2009, **131**, 3875–3877.
42 H. Liu, Y. Liu, Y. Li, Z. Tang and H. Jiang, *J. Phys. Chem. C*, 2010, **114**, 13362–13369.
43 B. Wang, A. P. Côté, H. Furukawa, M. O'Keeffe and O. M. Yaghi, *Nature*, 2008, **453**, 207–211.
44 G. Lu, S. Li, Z. Guo, O. K. Farha, B. G. Hauser, X. Qi, Y. Wang, X. Wang, S. Han, X. Liu, J. S. DuChene, H. Zhang, Q. Zhang, X. Chen, J. Ma, S. C. J. Loo, W. D. Wei, Y. Yang, J. T. Hupp and F. Huo, *Nat. Chem.*, 2012, **4**, 310–316.
45 R. Banerjee, A. Phan, B. Wang, C. Knobler, H. Furukawa, M. O'Keeffe and O. M. Yaghi, *Science*, 2008, **319**, 939–943.
46 Y. Hu, J. Liao, D. Wang and G. Li, *Anal. Chem.*, 2014, **86**, 3955–3963.
47 B. L. Cushing, V. L. Kolesnichenko and C. J. O'Connor, *Chem. Rev.*, 2004, **104**, 3893–3946.
48 H. Goesmann and C. Feldmann, *Angew. Chem., Int. Ed.*, 2010, **49**, 1362–1395.
49 S. Shylesh, V. Schünemann and W. R. Thiel, *Angew. Chem., Int. Ed.*, 2010, **49**, 3428–3459.
50 D. Wei and A. Ivaska, *Anal. Chim. Acta*, 2008, **607**, 126–135.
51 S. Upasham, I. K. Banga, B. Jagannath, A. Paul, K.-C. Lin, S. Muthukumar and S. Prasad, *Biosens. Bioelectron.*, 2020, 112940.
52 A. Paul, S. Muthukumar and S. Prasad, *J. Electrochem. Soc.*, 2020, **167**, 37511.
53 A. Bhide, B. Jagannath, A. Tanak, R. Willis and S. Prasad, *Sci. Rep.*, 2020, **10**, 2557.
54 A. M. O. Mohamed, P. Krokidas and I. G. Economou, *Mol. Syst. Des. Eng.*, 2020, **5**, 1230–1238.
55 K. Fujie and H. Kitagawa, *Coord. Chem. Rev.*, 2016, **307**, 382–390.
56 J. Qin, M. Cho and Y. Lee, *ACS Appl. Mater. Interfaces*, 2019, **11**, 11743–11748.
57 B. Koyuturk, C. Altintas, F. P. Kinik, S. Keskin and A. Uzun, *J. Phys. Chem. C*, 2017, **121**, 10370–10381.
58 I. Banga, A. Paul, S. Muthukumar and S. Prasad, *Sensors*, 2020, **20**, 1124.